Editors' Suggestion

Rare-Event Quantum Sensing Using Logical Qubits

Robert Ott,[1,2,*] Torsten V. Zache,[1,2] Soonwon Choi,[3] Adam M. Kaufman,[4] and Hannes Pichler[1,2]
[1]Institute for Theoretical Physics, University of Innsbruck, Innsbruck, 6020, Austria
[2]Institute for Quantum Optics and Quantum Information of the Austrian Academy of Sciences, Innsbruck, 6020, Austria
[3]Center for Theoretical Physics—a Leinweber Institute, Massachusetts Institute of Technology, Cambridge, Massachusetts 02139, USA
[4]JILA, University of Colorado and National Institute of Standards and Technology, and Department of Physics, University of Colorado, Boulder, Colorado 80309, USA

(Received 9 January 2026; accepted 18 August 2026; published 30 October 2026)

We present a novel protocol to detect rare signals in a noisy environment using quantum error correction (QEC). The key feature of our protocol is the discrimination between signal and noise through distinct higher-order correlations, realized by the nonlinear processing that occurs during syndrome extraction in QEC. In this scheme, QEC has two effects. First, it sacrifices part of the signal ϵ by recording a reduced, stochastic, logical phase $\phi_L = \mathcal{O}(\epsilon^3)$. Second, it corrects the physical noise and extends the (logical) coherence time for signal acquisition. For rare signals occurring at random times in the presence of local Markovian noise, we explicitly demonstrate an improved sensitivity of our approach over more conventional sensing strategies.

DOI: 10.1103/q4lp-htgw

Introduction—Quantum metrology [1–3] is one of the prime applications of quantum technologies [4–10]. By exploiting entanglement [11–19], quantum sensors can achieve sensitivities that improve linearly with the number of involved particles. This scaling is known as the "Heisenberg limit," and it constitutes a significant improvement over the "standard quantum limit" (SQL) reachable with uncorrelated probes. However, this conceptual advantage of entangled quantum sensors is typically rapidly lost in practical applications [20,21] due to decoherence [22–27].

While the same challenge arises in quantum computing [28–33], quantum error correction (QEC) [34] provides an efficient framework to protect quantum operations by encoding and monitoring quantum information in suitably entangled many-particle states. Accordingly, a natural question is whether quantum metrology might also benefit from analogous correction strategies [35–39]. Consideration of this question for Markovian noise reveals that, when the signal shares its operator structure with the noise—more precisely, if "the signal Hamiltonian lies in the span of the Lindblad or Kraus operators" [40–43]—QEC for quantum metrology is fundamentally limited: asymptotically, the sensitivity follows SQL scaling, and QEC is not helpful in many physical circumstances.

In this Letter, we present a novel type of quantum sensing protocol where QEC can enhance sensor performance for general local Markovian noise [Fig. 1(a)]. Our protocol applies to pulsed *collective* signals that are both *weak*, parametrized by a small-angle rotation ϵ, and *rare*, with a known, small, average pulse rate R; see Fig. 1(b) [44]. For such signals we demonstrate an advantage of our *logical* sensing strategy over standard *physical* sensing strategies when the physical noise rate γ dominates over the signal rate, i.e., $\gamma \gg R$. This is possible because the signal, after applying syndrome extraction and error correction, realizes a higher-order logical phase rotation [45–49] that can be coherently acquired. We show that, on average, our logical sensor behaves just like a physical sensor with renormalized signal strength and decoherence rates: while the error-correction procedure attenuates the signal strength from ϵ to ϵ^3, it also reduces the decoherence rate to allow for an extended sensing time of the logical sensors. This sensing time is the critical resource for improving the sensor sensitivity with QEC, and its extensions can more than offset the cubic reduction in signal. We demonstrate this behavior with analytical calculations and numerical simulations for the example of a [[7,1,3]] Steane code, and discuss generalizations to other codes further below.

Signal structure and sensing task—In this Letter, we consider a special type of signal consisting of short, randomly spaced pulses; see Fig. 1(b). We model the signal amplitude as $\omega(t) = \sum_i f(t - t_i)$, where each pulse has a shape f with pulse area $\epsilon = \int \mathrm{d}t f(t)$, and duration σ_t much shorter than all other relevant timescales, such that it is effectively described by a Dirac-delta function $f(t) = \epsilon\delta(t)$. To be concrete, we assume the pulses to arrive at random,

*Contact author: robert.ott@uibk.ac.at

Published by the American Physical Society under the terms of the Creative Commons Attribution 4.0 International license. Further distribution of this work must maintain attribution to the author(s) and the published article's title, journal citation, and DOI.

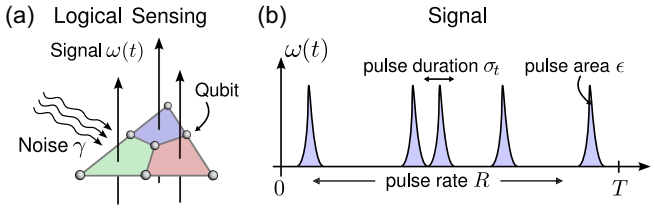

FIG. 1. QEC-enhanced logical sensing scheme. (a) We entangle physical sensors and form quantum codes—for example, a seven-qubit Steane code—to improve the sensing performance in the presence of local Markovian decoherence with strength γ. (b) We consider the task of sensing a random rare (with known rate R) and weak signal $\omega(t)$ in the form of short pulses with area ϵ and duration σ_t.

unknown times t_i, distributed according to a Poisson process with a known mean pulse rate R. In this setting, we consider the task of determining ϵ.

For this we consider a setup of n physical sensors that are exposed to the signal for a total sensing time T. We model the sensors as two-level systems, $\{|0\rangle_j, |1\rangle_j\}$, $j = 1, \ldots, n$, which couple homogeneously to the signal via the time-dependent Hamiltonian

$$H(t) = -[\omega(t)/2] \sum_{j=1}^{n} Z_j, \tag{1}$$

where Z_i are Pauli operators. We are interested in a weak signal limit, where each pulse imprints a small phase $\epsilon \ll 1$ [50], in the presence of local Markovian noise with strength γ. Here, we consider the case of dephasing noise, such that the Lindblad jump operators Z_i span the signal Hamiltonian. Thus, the qubits have a finite coherence time $\tau = 1/(2\gamma)$, which we assume to be much longer than a single pulse duration, $\tau \gg \sigma_t$. For such times $\gg \sigma_t$, the evolution is modeled with an effective master equation,

$$\partial_t \bar{\rho} = \gamma \mathcal{D}[\bar{\rho}] + R\mathcal{S}_\epsilon[\bar{\rho}], \qquad \mathcal{S}_\epsilon[\bar{\rho}] = U_\epsilon \bar{\rho} U_\epsilon^\dagger - \bar{\rho}, \tag{2}$$

for $\bar{\rho} = \langle\langle \rho \rangle\rangle$, where $\langle\langle \cdot \rangle\rangle$ denotes the ensemble average over the Poissonian signal process, $\mathcal{D}[\rho] = \sum_{j=1}^{n} (Z_j \rho Z_j - \rho)$, and the pulses act as a jump operator $U_\epsilon = \exp(i\epsilon \sum_{i=1}^{n} Z_i/2)$ representing collective phase kicks. Note that both signal and noise are therefore effectively described by nonunitary dynamics.

Physical (Ramsey) sensing—We first consider a standard Ramsey protocol with physical sensing qubits. For this, we may either prepare all n qubits independently (case R1), or in an entangled state (case R2). In the presence of noise, and for $\epsilon \ll 1/n$ [51], we choose optimal sensing intervals Δt, and both strategies (R1, R2) eventually give the same sensitivity, as the GHZ-state entanglement is fragile to noise [22]. The performance of estimating ϵ is given by the minimal uncertainty $\sigma_\epsilon = 1/\sqrt{F_{\mathrm{R}}^{\mathrm{tot}}}$, where $F_{\mathrm{R}}^{\mathrm{tot}}$ is the total quantum Fisher information (QFI) over multiple repetitions of the protocol [3]. In total, we get

$$F_{\mathrm{R}}^{\mathrm{tot}} = \frac{nR^2T}{4e\gamma}, \qquad \text{R1 and R2}, \tag{3}$$

with Euler number e; see Supplemental Material (SM) [52]. The Fisher information is proportional to the number of signal pulses RT, and additionally suppressed by the signal-to-noise ratio $R/\gamma \ll 1$. This quantifies the intuitive expectation that rare signals make it increasingly difficult to distinguish signal and noise background.

Classical error detection protocol—To eliminate noise, we next consider the sensors as a classical error-detecting code; see Fig. 2(b). Again, we distinguish the cases of n physical sensors without (case ED1) and with entanglement (case ED2). The sensors are exposed to both signal and noise for a very short sensing interval $\Delta t \ll 1/(n\gamma)$, after which we measure the individual observables X_i, $i = 1, \ldots, n$. Then we record measurement outcomes corresponding to two (or more) $X_i = -1$.

Overall, the probability for recording a signal scales as $p_2 \sim [n(n-1)/2](\epsilon/2)^4$ (ED1) and $p_2 \sim [(n/4)\epsilon]^4$ (ED2), which leads to the Fisher information (see SM [52]),

$$F_{\mathrm{ED}}^{\mathrm{tot}} = \begin{cases} (1/2)n(n-1)RT\epsilon^2, & \text{ED1}, \\ (1/16)n^4 RT\epsilon^2, & \text{ED2}. \end{cases} \tag{4}$$

Error detection has two effects: it filters the noise as multiple Z errors from dephasing are negligibly rare for $\Delta t \to 0$; however, it misses signal events and hence results in $F_{\mathrm{ED}}^{\mathrm{tot}} \propto \epsilon^2 \ll 1$. In the following, we demonstrate how this problem is overcome with our QEC-enhanced logical sensing strategy, which extends the logical coherence time τ_L far beyond the physical coherence time.

QEC-enhanced logical sensing—To illustrate our protocol, we first consider a single logical sensor constructed from seven qubits in a [[7,1,3]] Steane code, and discuss variants with multiple logical sensors later. While the

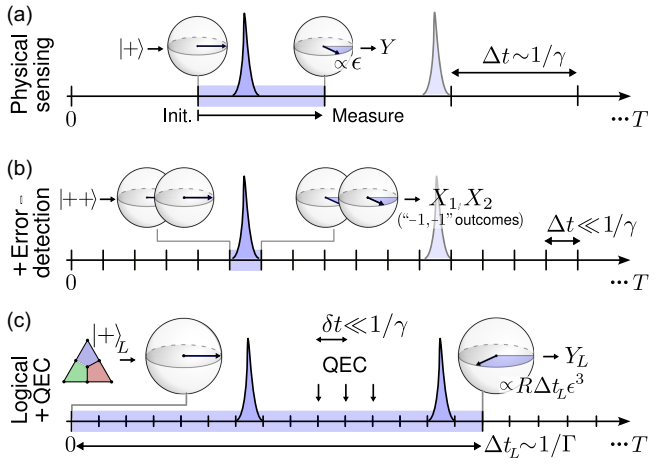

FIG. 2. Sensing strategies. We compare three different sensing strategies (see main text): (a) physical sensing (Ramsey); (b) physical sensing with classical error detection; (c) QEC-enhanced logical sensing. All three sensing strategies can be enhanced using entanglement between multiple physical or logical sensors.

numerical prefactors in the following expressions are specific to the Steane code, the overall scalings are general for distance-3 CSS codes.

Our operation cycle is sketched in Figs. 2(c) and 3(a): we perform a Ramsey sequence on the level of a logical qubit over the sensing interval Δt_L. That is, we initialize the qubits in the logical state $|\psi_L\rangle = |+_L\rangle = (|0_L\rangle + |1_L\rangle)/\sqrt{2}$, where $|0_L\rangle, |1_L\rangle$ are the logical basis states, and expose all physical sensors to the same signal (1), such that the real-time dynamics on the physical level is again described by Eq. (2). During this sensing interval, we perform repeated rounds of syndrome extraction in time steps δt, which we assume to be perfect without adding gate-level noise. The syndrome extraction rate must satisfy $\sigma_t \ll \delta t \ll \tau$ to efficiently correct the dephasing noise; it corrects for single-qubit errors, whereas higher-order errors result in a logical decoherence rate $\Gamma_\gamma = 42\gamma^2\delta t$. For simplicity, we assume that σ_t and δt are sufficiently short, such that signals and error correction operations never coincide.

However, while QEC at rate $\sim 1/\delta t$ corrects noise, it also removes part of the signal. To analyze this, we first consider how the signal interacts with the syndrome extraction rounds in a noise-free setting. That is, we consider an interval δt between two syndrome extraction events that contains a signal pulse described by the unitary operation $U_\epsilon = \exp(i\epsilon \sum_i Z_i/2)$ acting on the qubits. For distance $d = 3$ codes, this operator contains a logical signal in third order of ϵ. In the subsequent syndrome measurement, we distinguish two outcomes. With probability $p_+ \approx 1 - (7/4)\epsilon^2$, all stabilizers are measured with eigenvalue $+1$, and the measurement projects the state back into the code space $\mathcal{C}$. Importantly, as detailed in SM [52], this outcome results in the application of a logical phase gate with angle $\phi_L^+ \approx (7/4)\epsilon^3$. With probability $p_- \approx (7/4)\epsilon^2$, however, at least one stabilizer is flipped and the resulting state lies outside of the logical subspace $\mathcal{C}$. We then perform the usual error correction step to bring the state back into $\mathcal{C}$ [54]. As detailed in SM [52], this operation results in a logical phase gate with angle $\phi_L^- = -3\epsilon$. On average, per signal we thus obtain a logical phase with mean value $\phi_L = p_+\phi_L^+ + p_-\phi_L^- \approx -(7/2)\epsilon^3$ and variance $\sigma^2_{\phi_L} \approx \frac{63}{4}\epsilon^4$. Conversely, for intervals where no pulse appears, the syndrome extraction does not affect the logical state. In total, after a time interval Δt_L, which contains on average $R\Delta t_L$ signal pulses, the logical sensor acquires the mean logical phase $\Phi_L = (7/2)(R\Delta t_L)\epsilon^3$; see Fig. 3(c). The randomness associated with this signal acquisition with stochastic stabilizer outcomes (and their correspondingly different logical phases) results in dephasing of the logical phase given by $\sqrt{R\Delta t_L}\sigma_{\phi_L}$. This dynamics of our logical sensor is shown in Fig. 3(d), where we show individual trajectories (associated with the stochastic stabilizer outcomes) and corresponding ensemble averages and variances of the logical phase Φ_L.

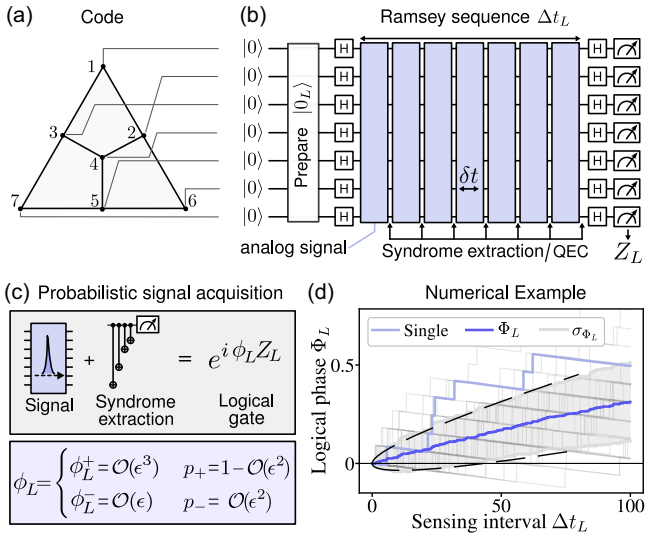

FIG. 3. Logical sensing protocol. (a) Our quantum sensor is built from quantum codes, e.g., a [[7,1,3]] Steane code. (b) QEC Ramsey cycle: we prepare the logical state $|+_L\rangle$, then sense the signal for a duration Δt_L interspersed with syndrome extraction in intervals of δt, and, finally, apply a logical projective measurement (at optimal bias point). (c) Syndrome extraction converts the signal to a probabilistic logical gate, with logical phase ϕ_L^+/ϕ_L^- depending on stabilizer outcomes with probabilities p_+/p_-. (d) Numerical demonstration of an average logical signal $\Phi_L \propto R\Delta t_L\epsilon^3$. We show data for $T = 100$, $\delta t = 10^{-3}$, $R = 30$, $\epsilon = 0.005 \times 2\pi$, $\gamma = 0$, and 50 runs; the dashed lines indicate the analytical estimate $\Phi_L \pm \sqrt{R\Delta t_L}\sigma_{\phi_L}$.

Extending this analysis of the logical sensor to include also the effect of dephasing noise, we find the following logical state after a number of $\Delta t_L/\delta t$ QEC cycles:

$$\rho_L(\Delta t_L) \approx \frac{1}{2}\begin{pmatrix} 1 & e^{(i\Omega-\Gamma)\Delta t_L} \\ e^{(-i\Omega-\Gamma)\Delta t_L} & 1 \end{pmatrix}, \tag{5}$$

written in the logical basis $\{|0_L\rangle, |1_L\rangle\}$ (see SM [52]), and we neglect terms of higher order in ϵ and $\gamma\delta t$. Here, we defined the logical signal strength $\Omega = \frac{7}{2}\epsilon^3 R$, and the logical decoherence rate $\Gamma = \Gamma_\gamma + \Gamma_R$, as the sum of $\Gamma_R = R\sigma^2_{\phi_L}/2 = \frac{63}{8}R\epsilon^4$, associated with the stochastic stabilizer outcomes, and $\Gamma_\gamma = 42\gamma^2\delta t$ associated with higher-order errors due to the physical noise. Since Γ_γ scales as $\sim\delta t$, it can be made arbitrarily small compared to Γ_R in the limit $\delta t \to 0$. In this limit, both the logical signal and decoherence rates scale as $\propto R$ [55]. For a logical measurement at the optimal bias point [Fig. 3(b)], the Fisher information with respect to ϵ is

$$F_L(\Delta t_L) = c(R\Delta t_L)^2\epsilon^4 e^{-2\Gamma\Delta t_L}, \tag{6}$$

where we have assumed $\gamma\delta t \ll \epsilon^2$, and defined a numerical constant $c = 9 \times 49/4$ specific to the Steane code. Equation (6) approximates the QFI of ρ_L to leading order once the mean logical phase exceeds its stochastic spread, $\Phi_L \gg \sqrt{R\Delta t_L}\sigma_{\phi_L}$ [Fig. 3(d)], i.e., for $\Delta t_L \gg 1/(R\epsilon^2)$, which includes the optimal sensing intervals discussed below

(see SM [52]). Equation (6) shows that $F_L \propto \epsilon^4$, which is a simple consequence of $F_L \propto [\partial\Omega/\partial\epsilon]^2$. This shows that logical sensors behave like single physical sensors but with renormalized signal $\epsilon R \to \epsilon^3 R$ and dephasing rates $\gamma \to \gamma^2 \delta t$.

Depending on the available total sensing time T we can distinguish two regimes. (i) If $T \ll 1/\Gamma$, it is optimal to perform a single sensing step over the full sensing time $\Delta t_L = T$. In this case, the sensitivity is determined via the resulting Fisher information $F_L^{\mathrm{tot}} = c(RT)^2\epsilon^4 + \mathcal{O}(\Gamma T)$. Comparison with the standard physical sensing strategy shows $F_L^{\mathrm{tot}}/F_{\mathrm{R}}^{\mathrm{tot}} \sim \epsilon^4 \gamma T$. Thus, sensitivity is enhanced by extending the sensing time as $T \gtrsim 1/(\gamma\epsilon^4)$ beyond the physical coherence time of the sensors. Similarly, comparing against error detection, we obtain $F_L/F_{\mathrm{ED}}^{\mathrm{tot}} \sim RT\epsilon^2$, which can be enhanced for sufficiently large sensing times $T \gtrsim 1/(R\epsilon^2)$. (ii) For even longer evolution times $T \gtrsim 1/\Gamma$, the optimal strategy is to repeat Ramsey cycles of duration Δt_L for a number of $M = T/\Delta t_L$ times, which yields the total Fisher information $F_L^{\mathrm{tot}} = MF_L(\Delta t_L)$. Optimizing sensing intervals as $\Delta t_L = 1/(2\Gamma)$ yields

$$F_L^{\mathrm{tot}} = c\frac{(R\epsilon^2)^2 T}{2\Gamma e} \xrightarrow{\delta t \to 0} c'\frac{RT}{e}, \tag{7}$$

with $c' = 7$. The optimal sensitivity in both regimes is shown in Fig. 4(a), and we compare against $MF_L(\Delta t_L)$ for different repetition numbers M.

In Figs. 4(b) and 4(c), we compare the sensitivities obtained from the different strategies in Eqs. (3), (4), and (7) [56]. Overall, we find an improved sensitivity of our logical sensing protocols when $\delta t \to 0$. Specifically, for a fixed number of available qubits, we find that $F_L^{\mathrm{tot}}/F_{\mathrm{R}}^{\mathrm{tot}} \to 4\gamma/R$, and $F_L^{\mathrm{tot}}/F_{\mathrm{ED}}^{\mathrm{tot}} \to 1/\epsilon^2$. This shows that the simultaneous renormalization of signal and dephasing rate due to QEC can have a net positive effect in either case: the advantage from the noise renormalization outweighs the (cubic) reduction of the signal. The underlying reason is that reduced decoherence with $\tau_L = 1/\Gamma \gg \tau$ allows to extend sensing time as the critical resource [57].

Multiple logically entangled sensors—Similar to physical sensors, our logical sensor can be enhanced by entangling n_L logical blocks. For this one considers the logical GHZ state, $|\psi_L\rangle = (|0_L\rangle^{\otimes n_L} + |1_L\rangle^{\otimes n_L})/\sqrt{2}$, and subsequently applies the sensing protocol to all n_L logical code blocks in parallel. If the total available sensing time is short, $T \ll 1/(n_L\Gamma)$, the optimal sensing interval is again $\Delta t_L = T$, where the extra factor n_L originates from the entanglement-enhanced logical decoherence rate. Otherwise, when $T \gtrsim 1/(n_L\Gamma)$, we set sensing intervals to $\Delta t_L = 1/(2n_L\Gamma)$. These strategies result in

$$F_L^{\mathrm{tot}} = \begin{cases} cn_L^2\epsilon^4(RT)^2, & T \ll \mathcal{O}[1/(n_L\Gamma)], \\ cn_L(R\epsilon^2)^2 T/(2\Gamma e), & T \gtrsim \mathcal{O}[1/(n_L\Gamma)]. \end{cases} \tag{8}$$

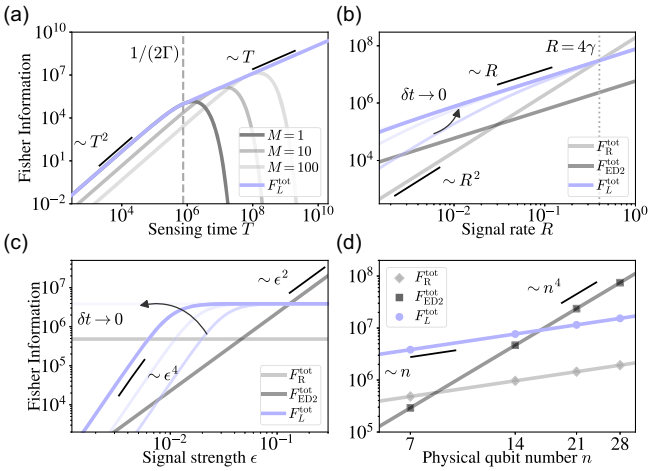

FIG. 4. Comparison of sensing strategies. (a) Logical Fisher information F_L^{tot} for $M = T/\Delta t_L$ repetitions. The blue curve is optimal for given total sensing time T and logical decoherence Γ. (b) Sensing performances versus signal rate R. Logical sensing outperforms physical sensing for small R and $\delta t \to 0$. (c) Sensitivities versus signal strength ϵ. For $\delta t \to 0$ and small ϵ, logical sensing outperforms physical sensing. (d) Dependence on physical qubit number n. Error detection yields the best asymptotic sensitivity scaling with n, versus n_L logical sensors with $n_L = n/7$. Parameters are chosen around $\gamma = 0.1, \epsilon = 0.036, n = 7, R = 0.05, \delta t = 10^{-8}, T = 3 \times 10^7$ [52].

This Fisher information gives rise to Heisenberg scaling for short evolution times T, where the sensitivity improves linearly in n_L and hence linearly in the number of physical sensors n. At larger times T, the advantage of entangling the n_L logical sensors is reduced to standard (SQL) scaling in n_L, analogous to the case of physical sensors [22]. While error detection can have better scaling in n [see Fig. 4(d)], logical sensing remains favorable for weak signals with $\epsilon \ll 1/n^2$ (and fast cycles δt). This may lead to advantages in scenarios where the number of sensing qubits is limited by technical constraints or spatial limitations, e.g., for nanoscale magnetic sensing [4].

Generalizations—Our logical quantum sensing scheme can be extended in several ways. First, we consider different error-correcting codes—for instance, a repetition code encoding one logical qubit into an odd number of d physical qubits. This changes the scaling relations of our protocol. Specifically, we obtain $F_L \sim (R\Delta t_L)^2\epsilon^{2(d-1)}\exp(-2\Gamma\Delta t_L)$, with the logical decoherence $\Gamma = \Gamma_\gamma + \Gamma_R$, $\Gamma_\gamma \sim \gamma(\gamma\delta t)^{(d-1)/2}$, and $\Gamma_R \sim R\epsilon^{d+1}$. For $\delta t \to 0$, this results in the total Fisher information, $F_L \sim RT\epsilon^{d-3}$. While this sensitivity is maximized for $d = 3$, larger distance can be beneficial for reaching the condition $\Gamma_\gamma/\Gamma_R \ll 1$ at a fixed δt, as the code corrects multiple errors. Furthermore, different codes imprint logical phases with different ϵ dependence, hence, combining codes allows for an independent estimation of ϵ and R, when R is unknown.

Second, we can include experimentally relevant noise models, e.g., quantum noise from spontaneous decay, which is a limiting factor for atomic clocks, as well as Markovian dephasing noise with spatial structure, such as global common-mode noise; see also Refs. [39,58–62].

Conclusions—Our sensing protocol transforms rare and weak transversal rotations into logical gates while preserving quantum coherence with QEC. Here, we explicitly exploit the spatiotemporal structure of the signal: the signal pulses simultaneously and collectively affect all sensor particles. Consequently, the signal generator U_ϵ can be distinguished from the Lindbladian noise operators in $\mathcal{D}$ through their higher-order dependence on ϵ. The QEC code performs the required nonlinear data processing that isolates and extracts these higher-order contributions, and using this, is able to outperform other more conventional strategies for this type of signal. Our protocol is, however, not in conflict with known results constraining the sensitivity of error-correction protocols when signal and noise couple to the sensor with the same operators [40–43]. In fact, the signal (2) defines a channel estimation problem, where the signal Hamiltonian lies in the span of Kraus operators [43], and the asymptotic QFI indeed scales linearly in sensing time and qubit number.

Our protocol further extends to general local Markovian noise with codes that correct such errors. Also note that, in general, our protocol requires active error correction, while for pure dephasing it suffices to only extract the syndromes.

A practical realization of our protocol is enabled by quantum systems with integrated error-correction capabilities, e.g., based on superconducting qubits, neutral atoms, or trapped ions; it will require fast and reliable quantum control and strong system-signal coupling, depending on the physical nature of the signal. For instance, our protocol can be advantageous for platforms with millisecond-scale syndrome extraction and coherent operation over several hours (SM [52]). While this is demanding, such conditions are potentially feasible in future atomic qubit platforms [63–67]. Eventually, however, the performance will be limited by gate-level noise of the quantum hardware in relation to the timescales of the physical signal. To conclude, it would be interesting to identify physical use cases of our protocol to probe rare and weak signals—for instance, in the context of dark matter detection [68] or gravitational wave astronomy [69], or, in combination with novel quantum-computing enhanced sensing schemes [70].

Acknowledgments—We thank Alexander Baumgärtner, Wolfgang Dür, Charles Fromonteil, Klemens Hammerer, Raphael Kaubrügger, Denis V. Vasilyev, and Peter Zoller for valuable discussions and feedback on the manuscript. This work is supported by the European Union's Horizon Europe research and innovation program under Grant Agreement No. 101113690 (PASQuanS2.1), the ERC Starting grant QARA (Grant No. 101041435), and the Austrian Science Fund (FWF) [Grant No. DOI 10.55776/COE1]. A. M. K. and H. P. acknowledge support from the NSF QLCI Award OMA-2016244, and A. M. K. support from the National Institute of Standards and Technology. S. C. acknowledges the support from the Sloan Research Fellowship and NSF via QuSeC-TAQS (OMA-2326787) and the Center for Ultracold Atoms, an NSF Physics Frontiers Center (PHY-1734011). In this work, Claude (Anthropic) and ChatGPT (OpenAI) were used to help check analytical formulas, choose plotting parameters for Figs. 4 and S1, prepare plotting code for Figs. 3(d), 4, and S1, and proofread the manuscript. The authors take full responsibility for the content.

Data availability—The data and code supporting the findings of this article are openly available in Zenodo [71].

[1] V. Giovannetti, S. Lloyd, and L. Maccone, Phys. Rev. Lett. **96**, 010401 (2006).
[2] C. L. Degen, F. Reinhard, and P. Cappellaro, Rev. Mod. Phys. **89**, 035002 (2017).
[3] L. Pezzè, A. Smerzi, M. K. Oberthaler, R. Schmied, and P. Treutlein, Rev. Mod. Phys. **90**, 035005 (2018).
[4] J. R. Maze, P. L. Stanwix, J. S. Hodges, S. Hong, J. M. Taylor, P. Cappellaro, L. Jiang, M. V. G. Dutt, E. Togan, A. Zibrov *et al.*, Nature (London) **455**, 644 (2008).
[5] N. Hinkley, J. A. Sherman, N. B. Phillips, M. Schioppo, N. D. Lemke, K. Beloy, M. Pizzocaro, C. W. Oates, and A. D. Ludlow, Science **341**, 1215 (2013).
[6] B. Bloom, T. Nicholson, J. Williams, S. Campbell, M. Bishof, X. Zhang, W. Zhang, S. Bromley, and J. Ye, Nature (London) **506**, 71 (2014).
[7] B. P. Abbott, R. Abbott, T. D. Abbott, M. R. Abernathy, F. Acernese, K. Ackley, C. Adams, T. Adams, P. Addesso, R. X. Adhikari *et al.*, Phys. Rev. Lett. **116**, 061102 (2016).
[8] R. H. Parker, C. Yu, W. Zhong, B. Estey, and H. Müller, Science **360**, 191 (2018).
[9] C. Overstreet, P. Asenbaum, J. Curti, M. Kim, and M. A. Kasevich, Science **375**, 226 (2022).
[10] F. Bonus, C. Knapp, C. Valahu, M. Mironiuc, S. Weidt, and W. Hensinger, Nat. Phys. **21**, 1189 (2025).
[11] T. Nagata, R. Okamoto, J. L. O'Brien, K. Sasaki, and S. Takeuchi, Science **316**, 726 (2007).
[12] C. Gross, T. Zibold, E. Nicklas, J. Esteve, and M. K. Oberthaler, Nature (London) **464**, 1165 (2010).
[13] I. D. Leroux, M. H. Schleier-Smith, and V. Vuletić, Phys. Rev. Lett. **104**, 073602 (2010).
[14] LIGO Scientific Collaboration, Nat. Phys. **7**, 962 (2011).
[15] W. Muessel, H. Strobel, D. Linnemann, D. B. Hume, and M. K. Oberthaler, Phys. Rev. Lett. **113**, 103004 (2014).
[16] D. Lachance-Quirion, S. P. Wolski, Y. Tabuchi, S. Kono, K. Usami, and Y. Nakamura, Science **367**, 425 (2020).
[17] K. A. Gilmore, M. Affolter, R. J. Lewis-Swan, D. Barberena, E. Jordan, A. M. Rey, and J. J. Bollinger, Science **373**, 673 (2021).
[18] W. J. Eckner, N. Darkwah Oppong, A. Cao, A. W. Young, W. R. Milner, J. M. Robinson, J. Ye, and A. M. Kaufman, Nature (London) **621**, 734 (2023).

[19] G. Bornet, G. Emperauger, C. Chen, B. Ye, M. Block, M. Bintz, J. A. Boyd, D. Barredo, T. Comparin, F. Mezzacapo *et al.*, Nature (London) **621**, 728 (2023).

[20] S. E. Crawford, R. A. Shugayev, H. P. Paudel, P. Lu, M. Syamlal, P. R. Ohodnicki, B. Chorpening, R. Gentry, and Y. Duan, Adv. Quantum Technol. **4**, 2100049 (2021).

[21] N. Aslam, H. Zhou, E. K. Urbach, M. J. Turner, R. L. Walsworth, M. D. Lukin, and H. Park, Nat. Rev. Phys. **5**, 157 (2023).

[22] S. F. Huelga, C. Macchiavello, T. Pellizzari, A. K. Ekert, M. B. Plenio, and J. I. Cirac, Phys. Rev. Lett. **79**, 3865 (1997).

[23] A. Fujiwara and H. Imai, J. Phys. A **41**, 255304 (2008).

[24] B. Escher, R. L. de Matos Filho, and L. Davidovich, Nat. Phys. **7**, 406 (2011).

[25] R. Demkowicz-Dobrzański, J. Kołodyński, and M. Guţá, Nat. Commun. **3**, 1063 (2012).

[26] R. Chaves, J. B. Brask, M. Markiewicz, J. Kołodyński, and A. Acín, Phys. Rev. Lett. **111**, 120401 (2013).

[27] R. Demkowicz-Dobrzański and L. Maccone, Phys. Rev. Lett. **113**, 250801 (2014).

[28] D. Bluvstein, S. J. Evered, A. A. Geim, S. H. Li, H. Zhou, T. Manovitz, S. Ebadi, M. Cain, M. Kalinowski, D. Hangleiter *et al.*, Nature (London) **626**, 58 (2024).

[29] Google Quantum AI and Collaborators, Nature (London) **638**, 920 (2025).

[30] B. L. Brock, S. Singh, A. Eickbusch, V. V. Sivak, A. Z. Ding, L. Frunzio, S. M. Girvin, and M. H. Devoret, Nature (London) **641**, 612 (2025).

[31] S. Krinner, N. Lacroix, A. Remm, A. Di Paolo, E. Genois, C. Leroux, C. Hellings, S. Lazar, F. Swiadek, J. Herrmann *et al.*, Nature (London) **605**, 669 (2022).

[32] P. Schindler, J. T. Barreiro, T. Monz, V. Nebendahl, D. Nigg, M. Chwalla, M. Hennrich, and R. Blatt, Science **332**, 1059 (2011).

[33] H. Putterman, K. Noh, C. T. Hann, G. S. MacCabe, S. Aghaeimeibodi, R. N. Patel, M. Lee, W. M. Jones, H. Moradinejad, R. Rodriguez *et al.*, Nature (London) **638**, 927 (2025).

[34] B. M. Terhal, Rev. Mod. Phys. **87**, 307 (2015).

[35] W. Dür, M. Skotiniotis, F. Fröwis, and B. Kraus, Phys. Rev. Lett. **112**, 080801 (2014).

[36] E. M. Kessler, I. Lovchinsky, A. O. Sushkov, and M. D. Lukin, Phys. Rev. Lett. **112**, 150802 (2014).

[37] G. Arrad, Y. Vinkler, D. Aharonov, and A. Retzker, Phys. Rev. Lett. **112**, 150801 (2014).

[38] T. Unden, P. Balasubramanian, D. Louzon, Y. Vinkler, M. B. Plenio, M. Markham, D. Twitchen, A. Stacey, I. Lovchinsky, A. O. Sushkov, M. D. Lukin, A. Retzker, B. Naydenov, L. P. McGuinness, and F. Jelezko, Phys. Rev. Lett. **116**, 230502 (2016).

[39] D. Layden, S. Zhou, P. Cappellaro, and L. Jiang, Phys. Rev. Lett. **122**, 040502 (2019).

[40] R. Demkowicz-Dobrzański, J. Czajkowski, and P. Sekatski, Phys. Rev. X **7**, 041009 (2017).

[41] P. Sekatski, M. Skotiniotis, J. Kołodyński, and W. Dür, Quantum **1**, 27 (2017).

[42] S. Zhou, M. Zhang, J. Preskill, and L. Jiang, Nat. Commun. **9**, 78 (2018).

[43] S. Zhou and L. Jiang, PRX Quantum **2**, 010343 (2021).

[44] This protocol targets the limiting case of extremely rare events, while generically, we do not expect to gain an advantage from logical sensing at large signal rates.

[45] Similar approaches have recently been explored to stochastically implementing small-angle transversal logical gates in quantum codes.

[46] E. Huang, P.-G. Rozon, A. Dua, S. Gopalakrishnan, and M. J. Gullans, arXiv:2510.01319.

[47] H. Choi, F. T. Chong, D. Englund, and Y. Ding, arXiv:2303.17380.

[48] R. Ismail, I. Chen, C. Zhao, R. Weiss, F. Liu, H. Zhou, S.-T. Wang, A. Sornborger, and M. Kornjača, PRX Quantum **7**, 020343 (2026).

[49] N. Yoshioka, A. Seif, A. Cross, and A. Javadi-Abhari, arXiv:2510.08290.

[50] The precise requirements on the size of ϵ will be clarified below.

[51] The sensitivity changes for $\epsilon \sim 1/n$, since, in that regime, sensing intervals with and without signal pulse can be distinguished with single shots with high success probability.

[52] See Supplemental Material http://link.aps.org/supplemental/10.1103/q4lp-htgw for further details, which includes Ref. [53].

[53] G. Last and M. Penrose, *Lectures on the Poisson Process* (Cambridge University Press, Cambridge, England, 2018), Vol. 7.

[54] In fact, it is not necessary to perform the error correction step; performing the syndrome measurements suffices.

[55] Of course, in practice, there is a lower limit for Γ set by the error-correction cycle time δt.

[56] In Figs. 4(b)–4(d), we evaluate Eq. (7) throughout. For small ϵ, the optimal sensing interval $1/(2\Gamma)$ can exceed the total sensing time T, such that a single sensing interval $\Delta t_L = T$ is optimal [regime (i)] and the achievable Fisher information is smaller. We neglect this effect here.

[57] Note that, in both cases, we are working in the many-pulse regime, where the number of pulses per logical sensing interval is large, i.e., $RT \gg 1$. Especially in the second case, (ii), this number can become so large that the average acquired phase $\Phi_L \sim 1/\epsilon$ exceeds 2π, which needs to be taken into account appropriately.

[58] D. Layden and P. Cappellaro, npj Quantum Inf. **4**, 30 (2018).

[59] P. Sekatski, S. Wölk, and W. Dür, Phys. Rev. Res. **2**, 023052 (2020).

[60] J. Bate, A. Hamann, M. Canteri, A. Winkler, Z. X. Koong, V. Krutyanskiy, W. Dür, and B. P. Lanyon, Phys. Rev. Lett. **135**, 220801 (2025).

[61] Y.-X. Wang, J. Bringewatt, A. Seif, A. J. Brady, C. Oh, and A. V. Gorshkov, arXiv:2410.05878.

[62] Such noise processes can also be addressed with decoherence-free subspaces.

[63] N.-C. Chiu, E. C. Trapp, J. Guo, M. H. Abobeih, L. M. Stewart, S. Hollerith, P. L. Stroganov, M. Kalinowski, A. A. Geim, S. J. Evered *et al.*, Nature (London) **646**, 1075 (2025).

[64] F. Gyger, M. Ammenwerth, R. Tao, H. Timme, S. Snigirev, I. Bloch, and J. Zeiher, Phys. Rev. Res. **6**, 033104 (2024).
[65] C. D. Bruzewicz, R. McConnell, J. Chiaverini, and J. M. Sage, Nat. Commun. **7**, 13005 (2016).
[66] J. A. Muniz *et al.*, arXiv:2506.09936.
[67] Y. Li, Y. Bao, M. Peper, C. Li, and J. D. Thompson, arXiv:2506.15633.
[68] D. F. Jackson Kimball and K. Van Bibber, *The Search for Ultralight Bosonic Dark Matter* (Springer Nature, Cham, Switzerland, 2023).
[69] C. Cahillane and G. Mansell, Galaxies **10**, 36 (2022).
[70] R. R. Allen, F. Machado, I. L. Chuang, H.-Y. Huang, and S. Choi, arXiv:2501.07625.
[71] R. Ott *et al.*, Rare-event sensing using logical qubits (data and code), Zenodo, 10.5281/zenodo.22961280 (2026).